Cytotoxicity of Metal and Semiconductor Nanoparticles Indicated by Cellular Micromotility

Marco Tarantola,[†] David Schneider,[†] Eva Sunnick,[†] Holger Adam,[†] Sebastien Pierrat,[†] Christina Rosman,[†] Vladimir Breus,[†] Carsten Sönnichsen,[†] Thomas Basché,[†] Joachim Wegener,[‡] and Andreas Janshoff[†,*]

[†]Institute of Physical Chemistry, University of Mainz, Jakob-Welder-Weg 11, 55128 Mainz, Germany, and [‡]Institute of Analytical Chemistry, Chemo- and Biosensors, University of Regensburg, Universitätsstr. 31, 93053 Regensburg, Germany

ABSTRACT In the growing field of nanotechnology, there is an urgent need to sensitively determine the toxicity of nanoparticles since many technical and medical applications are based on controlled exposure to particles, that is, as contrast agents or for drug delivery. Before the *in vivo* implementation, *in vitro* cell experiments are required to achieve a detailed knowledge of toxicity and biodegradation as a function of the nanoparticles' physical and chemical properties. In this study, we show that the micromotility of animal cells as monitored by electrical cell-substrate impedance analysis (ECIS) is highly suitable to quantify *in vitro* cytotoxicity of semiconductor quantum dots and gold nanorods. The method is validated by conventional cytotoxicity testing and accompanied by fluorescence and dark-field microscopy to visualize changes in the cytoskeleton integrity and to determine the location of the particles within the cell.

KEYWORDS: epithelial cells · ECIS · micromotion · transepithelial resistance (TER) · cytotoxicity · gold nanorods · multishell quantum dots

In the last years, nanoscale objects with dimensions in the range of 1 to 100 nm became ubiquitous, and these nanomaterials are released from a variety of sources such as common industrial or consumer products. As a consequence, the environment is exposed to particles of variable origin cast in the atmosphere, water, and soil. Human exposure to nanomaterials occurs most likely during manufacturing processes, but inhalation of nanomaterials released to the atmosphere and ingestion of water or food may also be possible.[1] Dermal exposure from various sources such as sunscreen might also be likely.[2] These circumstances call for effective and reliable screening assays capable of reporting the response of cells to the exposure to nanoscale particles (NPs). Conventional cytotoxicity assays address the cellular metabolic activity like the 3-(4,5-dimethylthiazol-2-yl)-2,5 diphenyl tetrazolium bromide test (MTT), the integrity of the cellular plasma membranes (*e.g.*, lactate-dehydrogenase (LDH) release assay), or the activity of intracellular housekeeping enzymes (Calcein acetoxymethyl ester). These tests are time-consuming, invasive, and crude as far as the amount of information is concerned. Moreover, many colorimetric or fluorescence-based approaches to quantify cytotoxicity are impaired by the presence of the nanoparticles in the test tube and their peculiar optical properties (*e.g.*, autofluorescence, fluorescence quenching, light scattering). Hence, alternative label-free and—for the purpose of dynamic toxicity screening—noninvasive methods are required to meet the growing demand of vast and versatile cytotoxicity assays[3] that permit a quick assessment of the impact of nanomaterials on various cell types.

In this study, label-free and noninvasive AC impedance measurements have been used to quantify the impact of nanoparticles on the viability of adherent cells. The general approach to monitor adherent cells by impedance measurements is referred to as electric cell-substrate impedance sensing (ECIS), and it has been first described by Giaever and Keese.[4] In the ECIS setup, the cells are grown on planar gold-film electrodes that are deposited on the surface of a cell culture vessel. The impedance of these electrodes increases when animal cells adhere and spread on the surface of these electrodes until a confluent cell monolayer is formed (Figure 1). In confluent cell layers, the measured impedance is not a constant value but changes whenever the shape of the cells or the cell−cell junctions change as the dimensions of the current pathways around the cells bodies are altered (see Figure 1). As cell shape and the cell−cell junctions determine the impedance readout, ECIS has found a broad range of applications in biomedical research from simple measurements of cell adhesion to studies

*Address correspondence to janshoff@uni-mainz.de.

Received for review October 30, 2008 and accepted December 03, 2008.

Published online December 18, 2008. 10.1021/nn800721j CCC: $40.75

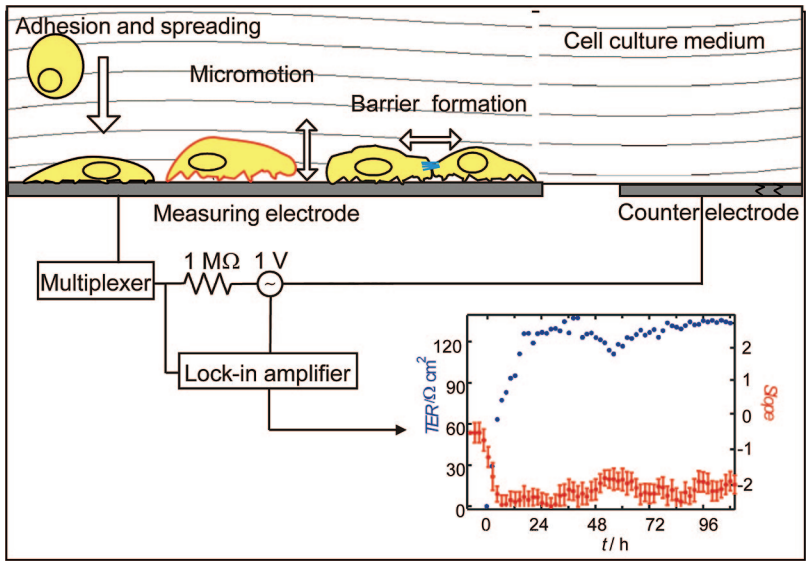

Figure 1. Experimental setup (based on ref 9): The graph shows both the transepithelial restistance TER recorded between 10 and 10^4 Hz (blue circles) and the slope (red circles) of the Fourier analysis of micromotion recorded at 4 kHz as a function of time. Cell seeding was at 0 h.

addressing the invasion of metastatic cancer cells *in vitro*. It has also been successfully applied to monitor cytotoxicity of various chemical or biological challenges.[5−8] In all studies, ECIS results were reported to be in closest agreement with classical cytotoxicity approaches as mentioned above but provide time-resolved information without the need to label the cells.

One special mode of ECIS measurements records the complex impedance of the cell-covered electrodes at one fixed AC frequency with very high time resolution (<1 s). The observed fluctuation of the signal mirrors the fluctuations of the three-dimensional shape of the cells on the electrode surface. These fluctuations in cell shape have been termed *micromotion*. Micromotion is completely and irreversibly suppressed when the cells are exposed to formalin,[9] which is well-known to cross-link all cellular proteins. By comparing the degree of micromotion as a function of temperature or glucose supply, Lo *et al.* were able to correlate micromotion to the metabolic activity of the cells and their overall viability.[10] Recently, ECIS-based micromotion measurements were evaluated as a possible indicator to distinguish cancerous from noncancerous cell lines due to their different motility.[11]

The present work reports on repeated micromotion measurements on epithelial MDCK (type II) cells, which are continuously exposed to increasing amounts of colloidal semiconductor quantum dots (QDs) and gold nanorods. MDCK cells are an established and well-characterized model system for barrier forming epithelial cell lines. Micromotion results were validated by conventional MTS cytotoxicity assays and supported by microscopic studies addressing cytoskeletal integrity after NP exposure. Two kinds of particles have been studied: gold nanorods with a mean size of 17 by 39 nm and CdSe/CdS/ZnCdS/ZnS multishell QDs with a diameter of 5−6 nm. Rod-shaped gold nanoparticles show extremely high polarizability at the plasmon frequency and are thus useful as contrast agents in biomedical imaging and as photothermal transducers for localized hyperthermia therapies. In the latter, the idea is to bind them specifically to designated target cells by appropriate surface modification and subsequently to heat them using their strong light absorption in the near-infrared.[12] Semiconductor QDs are well-suited for fluorescent labeling and single particle tracking. In fact, due to their photostability, QDs are already frequently used as biomarkers *in vitro* and *in vivo*.[13,14]

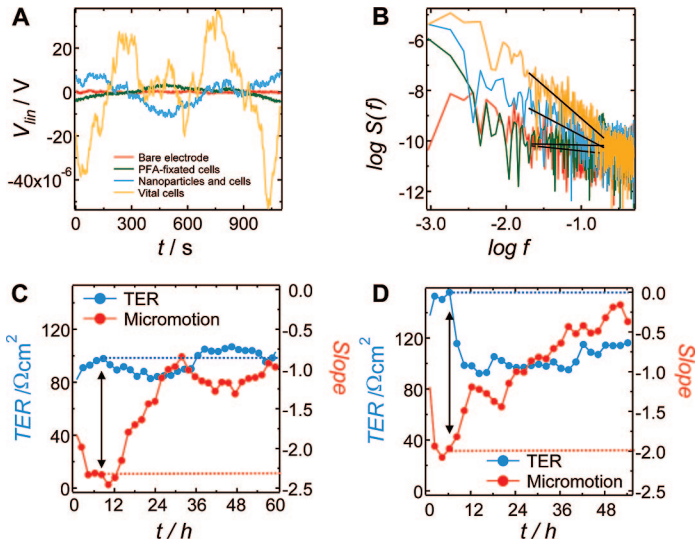

Figure 2. (A) In-phase voltage fluctuations (micromotion raw data) under various load situations. The highest fluctuation amplitude is found for living untreated cells (yellow), while cells exposed to nanoparticles exhibit significantly lower micromotion (blue). Fixated cells (green) and cell-free gold electrodes (red) display merely digital noise. (B) Power spectral densities under the corresponding load situations: empty electrodes (red) and fixated cells (green) show a slope close to zero, while motility (yellow) of vital cells provides an average slope of −2.6. Addition of CTAB-coated gold nanorods results in a reduction of motility (blue) expressed by a slope of approximately −1. (C) Transepithelial resistance (TER) (blue) and micromotion slope (red) after addition of 7.5×10^{13} p/mL QDs as a function of time. (D) Time course of TER (blue) and micromotion slope (red) after addition of 1.38×10^{11} p/mL CTAB gold nanorods. Time upon reaching confluency is set to zero.

RESULTS AND DISCUSSION

Micromotion as an Indicator for Nanoparticle Cytotoxicty. Our aim was to elucidate whether the fluctuations in the real part of the impedance caused by the metabolically driven shape fluctuations of confluent cells adhered to the surface of a gold microelectrode (Figure 2A,B) can serve as an indicator for dose-dependent cytotoxicity of nanoparticles.

Micromotion (Figure 2A) raw data was Fourier transformed (Figure 2B) to produce power density spectra. The slope m from the low frequency regime (Figure 2B) serves as a quantitative measure to what extent the adherent cells are vital.[10] As a first reference and control, 4% (v/v) paraformaldehyde-fixated cells showing no residual motility were employed.

Figure 2C,D shows the degree of micromotion, quantified by the slope of the power spectrum, as a function of time when confluent MDCK II cells are exposed to QDs (Figure 2C) or gold nanorods coated with detergent cetyl triammonium bromide (CTAB) to stabilize the particles in solution (Figure 2D) (addition time marked with arrows). Besides the slope of the power density m, we also plotted the time course of the transepithelial resistance TER. The TER, which is a measure for the tightness of cell−cell junctions,[15] is only meaningful when a confluent, fully formed monolayer has been established which coincides with full micromotion that is typically characterized by a slope of the power density of $m \approx -2.5$ (Figure 1, inset). Nanoparticles were only added after equilibrium values for TER and m had been reached. Time courses of the power density slopes m show a continuous increase (from -2.5 to -1) upon the addition of both types of nanoparticles to the established cell monolayer, starting after 2 h of incubation, which is indicative of a reduction of cell motility with exposure time (Figure 2C,D); the standard deviation of the slope is around ± -0.2. However, the time courses of the transepithelial resistance TER do not show a significant change during particle exposure for the QD concentrations (7.5×10^{13} p/mL) (Figure 2C) used here and one-third of reduction (from 150 to 100 Ωcm^2) for gold nanoparticle concentrations of 1.38×10^{11} p/mL (Figure 2D). Hence, we conclude that micromotion is a better suited indicator for the onset of cytotoxicity than TER monitoring. Apparently, MDCK cells show a significant alteration of their metabolically driven motility before their predominant physiological function to serve as an interfacial tissue is compromised.

Typical time courses of normalized micromotion values are depicted in Figure 3 for four kinds of nanoparticles (QD, gold nanorods either coated with CTAB, PEG-NH_2, or PEG-COOH) and the two components that may be released from the individual particles—CTAB and Cd^{2+}—for control purposes. Exemplary, four different concentrations are shown, but for the sake of clarity, only the highest concentration was subjected to an empirical sigmoidal fit. Results for the two controls, either untreated cells or cell-free electrodes, are included in the diagrams. For standardization, the slope $m(t)$ is corrected by the mean values of the cell-free-electrode control $\langle N \rangle$ and related to the slope originated from untreated cells $\langle M \rangle - \langle N \rangle$ for each well (eq 1):

$$W(t) = \frac{m(t) - \langle N \rangle}{\langle M \rangle - \langle N \rangle} \times 100 \qquad (1)$$

The standard deviation of m (not shown) is about 10% in all experiments. All $W(t)$ data sets were smoothed with adjacent averaging over four consecutive values, and the experiments were conducted more than two times with a standard deviation of 10%, indicating good reproducibility.

QDs and CTAB-coated gold rods (Figure 3A,B) at particle concentration of 3×10^{14} QDs (p/mL) and 1.38×10^{11} CTAB rods (p/mL) reduce cell motility of the confluent MDCK II monolayer drastically, while low concentrations of 4×10^{12} (QDs) or 4.6×10^{9} (CTAB rods) p/mL show no influence on cell motility. A substantial recovery of micromotion at medium particle concentrations (*i.e.*, 2.4×10^{14} for the semiconductor ones or 1.02×10^{11} for the metallic ones) was found, which can be attributed to adaptation of the epithelial kidney cell lines,

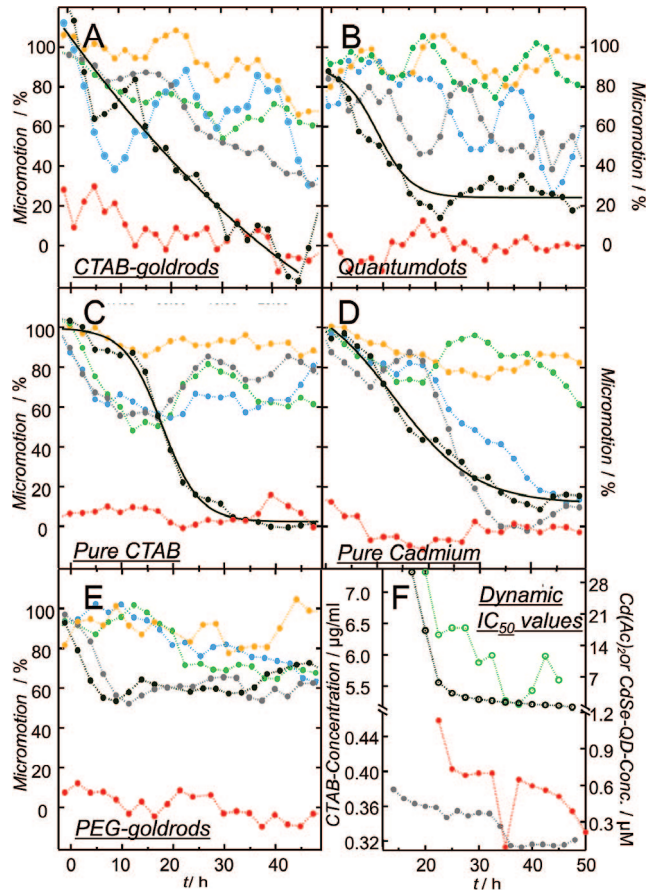

Figure 3. Micromotion of living cells (yellow) and bare electrode signal (red) as a function of nanoparticle exposure. (A) CTAB gold nanorods (in p/mL): 1.38×10^{11} (black), 1.02×10^{11} (gray), 6.6×10^{10} (blue), 4.6×10^{9} (green). (B) QDs (in p/mL): 3×10^{14} (black), 2.4×10^{14} (gray), 1.5×10^{14} (blue), 4×10^{12} (green). (C) Pure CTAB (in µM): 31.25 (black), 6.25 (gray), 3.125 (blue), 0.625 (green). (D) Pure cadmium ($CdAc_2$ in µM): 31.25 (black), 6.25 (gray), 3.125 (blue), 0.156 (green). (E) PEGylated gold nanorods (in p/mL): 1.38×10^{11} (black), 4.6×10^{11} (gray), COOH-terminated rods; 1.38×10^{11} (blue), 4.6×10^{11} (green), NH_2-terminated PEG rods. (F) Dynamic IC_{50} values determined from micromotion: CTAB concentration on nanorods (red), free CTAB (in µg/mL) (green), QDs (gray), and $CdAc_2$ (black) (in µM).

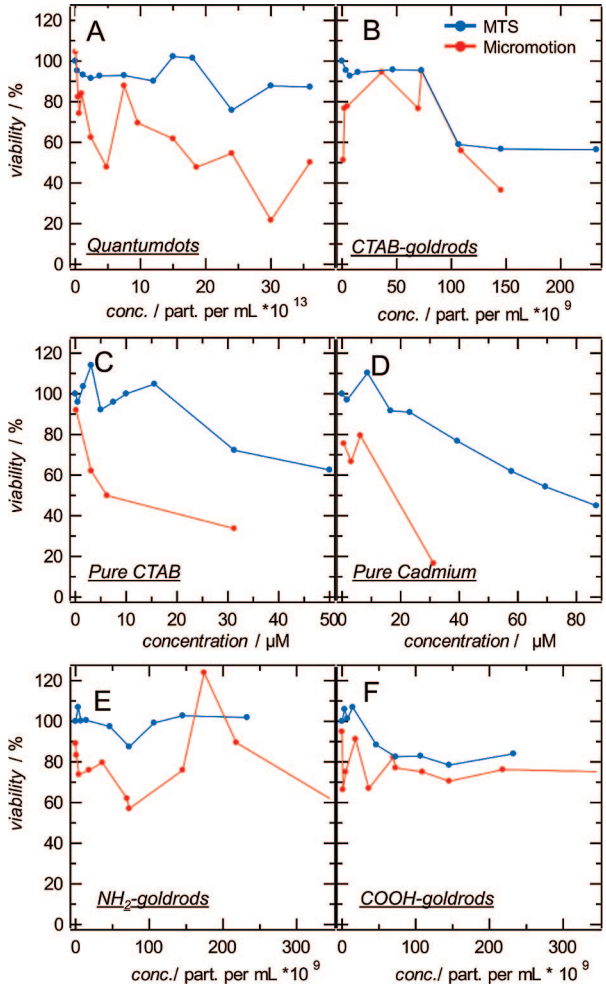

Figure 4. Comparison of cell viability determined by micromotion (red) and by the conventional MTS test (blue). Graphs depict viability as a function of concentrations: (A) multishell quantum dots, (B) CTAB gold nanorods, (C) pure CTAB, (D) pure $CdAc_2$, (E) NH_2—PEG gold rods, (F) COOH-PEG gold nanorods.

although this recovery effect was short termed in the case of QDs (6—8 h as compared to full recovery for gold particles). We found that, at intermediate concentrations, cells recover twice as fast from particle treatment as from addition of pure CTAB solution. Addition of $CdAc_2$, however, did not result in viability recovery within the observation time scale (Figure 3C,D). At the same time, microscopic images (phase contrast) showed no evidence for cell detachment on the measuring electrode, so we can exclude that the observed recovery is caused by cell proliferation and replacement of dead cells. Importantly, substitution of the CTAB layer surrounding the gold nanorods by amino-terminated polyethylenglycol leads to full cytocompatibility over the monitored 48 h interval up to a particle concentration of 1.32×10^{12} p/mL (Figure 3E, shown for 4.6×10^{11} p/mL). The untreated cell population and those treated with NH_2—PEG nanoparticles are virtually indistinguishable, confirming the expected "stealth" character of the PEG coating.[16] However, using carboxy-terminated PEG as a coating for gold nanorods resulted in a decrease in micromotion almost down to 50% within the first 24 h of incubation followed by a slow recovery to nearly 60%. The results contradict observations by Goodman *et al.*;[17] in their study, quaternary ammonium groups on monolayer-coated gold clusters showed a considerable toxicity, while nanoparticles functionalized with negatively charged side chains revealed no toxicity. Figure 3F stresses one of the advantages of impedance measurements over classical, end-point cytotoxicity tests. ECIS allows monitoring of the dynamic IC_{50} value, that is, the individual IC_{50} values after different exposure times. For this purpose, the particle concentration at half-maximum micromotion was determined for increasing exposure times. For comparison, concentrations of QD particles and $CdAc_2$ are given in micromolar, CTAB concentration surrounding the CTAB gold particles as well as the pure CTAB in solution in micrograms per milliliter.

In general, the dynamic IC_{50} decreases with increasing time, as one would expect. However, for QDs, scaled in micromolar, we found a biphasic decrease of the dynamic IC_{50} with a plateau phase around 20 h exposure times with an IC_{50} of 350 nM. This behavior is indicative of a fast toxic effect at concentrations higher than 350 nM, equivalent to 2×10^{14} p/mL after addition, followed by a slower process with significant lower IC_{50} below 100 nM. We attribute this biphasic behavior to a quick response of cells to the uptake of QD and a delayed answer to washing out of toxic cadmium ions from the QD particles. The delay can be explained by the diffusion barrier provided by the multishell arrangement, as reported by Kirchner *et al.*[18] Cadmium ions from solution display a faster response of the micromotion assay, as expected due to its immediate availability.

As far as the toxicity of CTAB-coated gold nanorods expressed in IC_{50} value is concerned, we refer to it in Figure 4 and Table 1. In Figure 3F for dynamic IC_{50} values instead, we show that pure CTAB added from solu-

TABLE 1. IC_{50} Values after 24 and 48 h Determined by Micromotion and MTS

nanoparticle or toxin	IC_{50} micromotion$_{24\ h}$	IC_{50} MTS$_{24\ h}$	IC_{50}micromotion$_{48\ h}$	IC_{50}MTS$_{48\ h}$
pure CTAB (µM)	6.4	111.2	5.5	16.5
pure $Cd(Ac)_2$ (µM)	4.3	73.9	0.3	nontoxic up to 0.3
CTAB rods (p/mL)	1.20×10^{11}	nontoxic up to 2.30×10^{11}	8.5×10^{10}	8.75×10^{10}
multishell QDs (p/mL)	2×10^{14}	nontoxic up to 4×10^{14}	1×10^{14}	190×10^{14}
COOH—PEG rods (p/mL)			nontoxic up to 1.32×10^{12} in 2.2 days	
NH_2—PEG rods (p/mL)			nontoxic up to 1.32×10^{12} in 2.5 days	

tion affects micromotion to a smaller extent than the same concentration of CTAB found on the coated particles.

We determined the amount of CTAB attached to the gold particles by thermal gravimetric analysis (TGA, 24 μg CTAB/mg gold, indicating a bilayer of CTAB surrounding a single rod) to find out to what extent toxicity is influenced by the uptake and presence of particles as compared to pure CTAB. We found 20-fold lower dynamic IC_{50} values for a CTAB-coated particle as neat CTAB solution. From this, we conclude that either the particles are toxic or the amount of membrane-active CTAB within the cells is higher if the particles were used as carriers.[19] The latter finding is supported by our observation that CTAB-coated particles show the tendency to form clusters once taken up by the cell (data not shown).

Comparison of Micromotion with Conventional MTS Assay. The noninvasive micromotion assay is validated by the established MTS test. For this purpose, the time courses of resistance fluctuations are recorded for various concentrations of different particles and free cadmium acetate and pure CTAB. We compared the viability measured through micromotion under identical conditions (exposure time and particle concentration) with the viability readings provided by the MTS test (Figure 4). Experiments were carried out in triplicate. Cell viability determined by MTS and micromotion are determined after 24 h of exposure of the cell to the particles. We found good agreement between both assays, although with bigger fluctuations in the ECIS assay, as far as the general trend is concerned; however, the micromotion assay shows a significant higher sensitivity than the MTS test since it responds already at lower particle concentration. IC_{50} values for both assays are compiled in Table 1 for the 24 and 48 h exposure time. The micromotion assay reports approximately 20-fold lower IC_{50} values for the two chemicals (CTAB and $CdAc_2$) and 2−4-fold lower values for the nanoparticles after 24 h intervals compared to MTS tests. After 48 h, the IC_{50} values are closer together, although the highly toxic QDs produce a 200-fold lower IC_{50} in the micromotion assay as compared to the MTS test. The discrepancy in sensitivity between the micromotion assay and the MTS test is even more pronounced if confluent cells were used for the MTS test instead of subconfluent cells.[20] Confluent cells in the MTS test result in 20% higher IC_{50} values (data not shown) as compared to subconfluent ones (Table 1).

Regarding the analytical performance of impedance-based measurement of cellular micromotility, it should be noted that this assay can be applied to all adherent cells that show measurable fluctuations in their cell shape. Micromotion should be clearly distinguished from measurements on cellular migration which involves lateral movement of the cell body into an open space on the culture substrate. In micromotion experiments as performed here, we used confluent cell layers such that the readout reports more on shape fluctuations rather than cell movement. Micromotion readings have been reported for several different adherent cell types before. It was shown that the recorded impedance fluctuations are metabolically driven and mediated by the cytoskeleton. In a very recent paper,[21] Lovelady *et al.* could show that micromotion readings on 3T3 fibroblasts report on cellular changes for levels of toxin exposure that have previously not been considered as being harmful. Moreover, different cell types show a very individual pattern in the time course of impedance fluctuations, for instance, with respect to long-range and short-range fluctuations. However, this latter point is also a weak spot of the assay that it shares with other cytotoxicity assays. Measurements with different cell types, with individual levels of micromotion under control conditions, suffer from the problem of correct normalization for this individual noise signature. Simple use of relative fluctuation changes might be an oversimplified way to deal with this problem. In most studies, however, a direct comparison of micromotion levels is not very relevant. Also, ECIS-based micromotion readings are clearly a holistic approach to read cytotoxicity. For instance, we cannot distinguish between *apoptosis* and *necrosis* as the cause for cell death from ECIS readings today as other assays based on molecular recognition might. However, these have shown to be less sensitive.[22]

Localization of Nanoparticles and Visualization of the Cytoskeleton by Optical Microscopy. Both the MTS and micromotion assays are quantitative but functional tests. Cytotoxicity of nanoparticles depends heavily on the uptake of the particles into the cell, that is, the concentration of particles in the cytosol or any intracellular compartment. Thus, we addressed the question whether the different particles enter the cells to different degrees and where they are located inside the cell. While gold nanorods are visualized within the cells by dark-field microscopy making use of their plasmonic resonance, QDs are readily imaged by fluorescence microscopy. Since micromotion relies on an intact cytoskeleton, we also stained the Actin and microtubule network using different particle concentrations and exposure times. In Figure 5a, fluorescence micrographs of Actin stained with Alexa-labeled phalloidin (1, 2, 5, and 6) as well as Alexa-labeled IgG_1 specific for β-tubulin (3, 4, 7, and 8) are compared for different incubation times and particle concentrations. The immunofluorescence of the control upon reaching confluency (0 h, Figure 5a, 1 and 3) and after 48 h (Figure 5a, 2 and 4) without particles shows typical intracellular Actin filaments and microtubules: f-Actin fibers, a cortical ring, tubules, and β-tubulin monomeres in vesicles. After 48 h, cells occupy a smaller area and bundles of Actin as well as small internal aggregates can be found, while microtubules are too dense to distinguish single

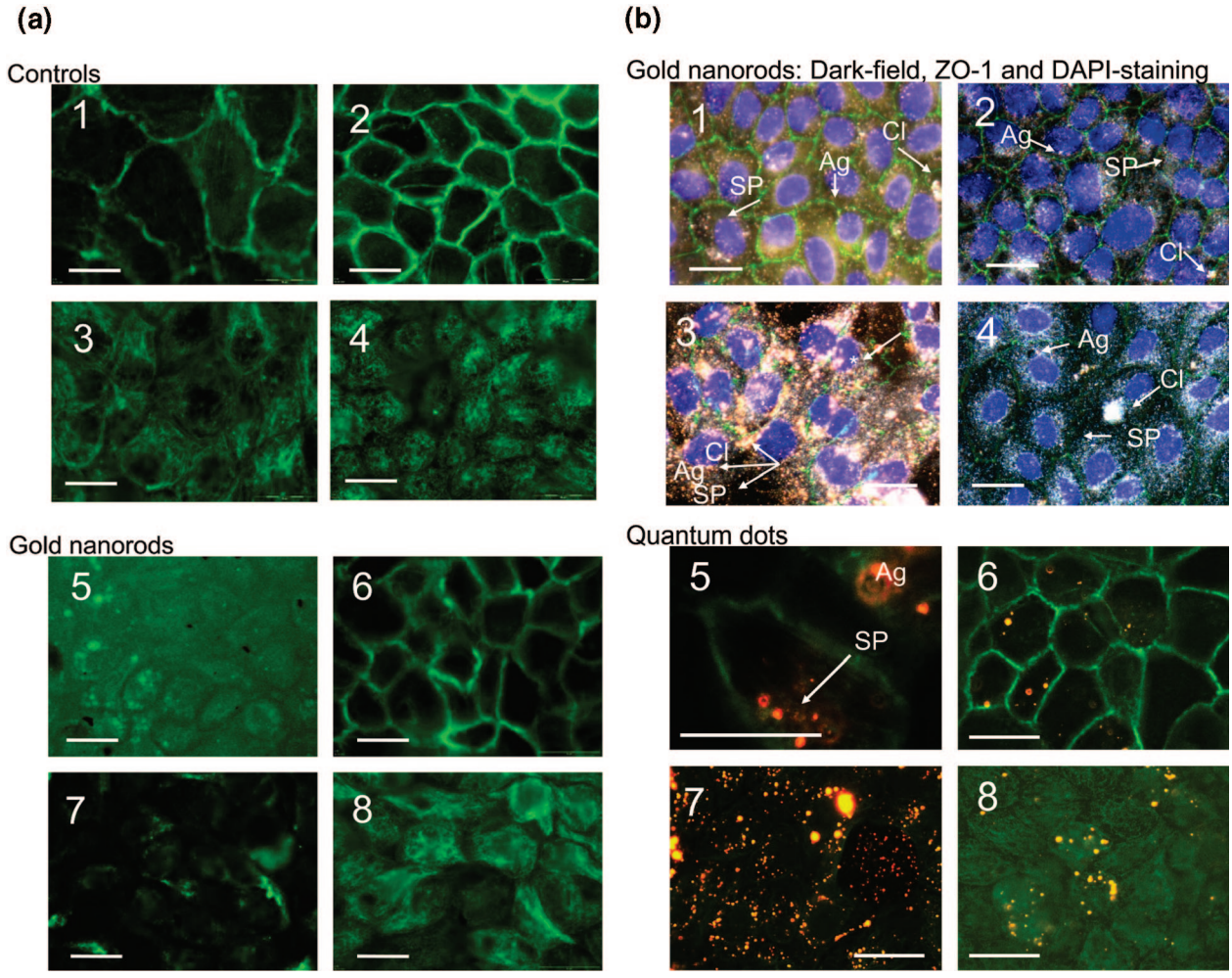

Figure 5. (a) Fluorescence light microscopic images after staining of Actin (first and third row) or microtubules (second and fourth row). 1−4: Controls after 24 h upon attaining confluency (t = 0) (1 and 3) and 48 h after reaching confluency (2 and 4) without nanoparticles. 5−8: Micrographs after 48 h of incubation with 1.38 × 10^{11} p/mL gold nanorods (5 and 7, CTAB; 6 and 8, NH_2−PEG). Scale bar is 20 μm. (b) 1−4: Overlay of dark-field images and fluorescence images with ZO-1 and nucleus staining after 48 h incubation with (1) 4.6 × 10^{10} or (3) 6.6 × 10^{11} CTAB rods as well as (2) COOH−PEG gold nanorods and (4) NH_2−PEG gold nanorods (1.32 × 10^{12} p/mL); arrows pointing at single particles (SP), aggregates of 2−20 particles (Ag), or clusters (20 and more particles). Additionally (under 3), discontinuous ZO-1 staining (*) is highlighted. 5−8: Fluorescence image of MDCK cells after 24 h of incubation with multishell quantum dots at two concentrations: 3.75 × 10^{14} (5 and 7) and 1.9 × 10^{14} p/mL (6 and 8). Arrow in 1 is pointing at single particles aligned with Actin fibers. Scale bar is 20 μm.

tubules anymore. Figure 5a, 5−8, shows a cell monolayer after addition of 1.38 × 10^{11} gold nanoparticles (5 and 7 coated with CTAB, 6 and 8 with NH_2−PEG) and after a 48 h incubation time. Cells exposed to CTAB rods show gaps between adjacent cells in the Actin staining (corresponding to reduced TER recordings), where the cortical ring used to be, while unusual aggregates of Actin occur in the cytosol (Figure 5a, 5). β-Tubulin is redistributed in monomers to the cell periphery, and cells are generally diminished in size (Figure 5a, 7). In contrast, PEGylated particles do not show any visible changes in the cells' cytoskeleton (Figure 5a, 6 and 8).

We also managed to localize the gold nanoparticles in or outside the cells by means of dark-field microscopy. In order to improve the precision of particle localization, we co-stained both the nucleus by DAPI and the tight junctions by ZO-1 staining (Figure 5b, 1−4). The particles are easily identified by the orange to red color originating from localized plasmon resonance. Notably, up to 20% of the solution consists of spherical gold particles that appear green in the scattered light. Generally, we found that the particles, regardless of their coating, preferably arrange around the nucleus without entering it, which has also been reported previously.[23]

While CTAB-coated gold nanorods accumulate in the cytosol already at low particle concentrations, we found substantially less particles with PEG coatings within the cells. At low particle concentration (4.6 × 10^{10} p/mL), individual CTAB-coated nanorods and many aggregates are distinguishable without affecting cell−cell boundaries (Figure 5b, image 1). By moving the focal plane, we made sure that the particles are indeed in the cytosol and not above or beneath the cells. At higher particle concentrations (6.6 × 10^{11} p/mL, Figure 5b, image 3), CTAB rods tend to form larger aggre-

gates and the cell−cell boundaries are destroyed, accompanied by partial cell detachment.

Figure 5b, images 2 and 4, shows the results of cells exposed to PEG-coated gold particles (with NH_2 or COOH groups; 1.32×10^{12} p/mL); it can be seen that nuclei are unaffected and ZO-1 staining is continuous. Comparing image 1 (CTAB) with image 2 (COOH−PEG), we find that roughly the same amount of gold nanorods is found in the cytosol, although the first ones are aggregated and the latter are not. However, for PEGylated particles (COOH), a 10-fold higher concentration was necessary to achieve the same particle density in the cells. Although our findings confirm the nontoxic nature of PEGylated particles, which enter the cells less efficiently but do not alter their internal structure (cytoskeleton, nucleus, cell−cell boundaries), particle uptake is reduced by roughly a factor of 10 compared to that of CTAB-coated particles.

In Figure 5b, 5−8, the impact of two different QDs concentrations, 3.75×10^{14} and 1.9×10^{14} p/mL, on confluent MDCK II cells is shown. At higher particle concentration, particle aggregates within the cells as well as cell desorption from the surface occur (Figure 5b, images 5 and 7), while at lower concentration (Figure 5b, images 6 and 8), which has been used for the micromotion assay, no effect on the cell layer integrity is found. Cadmium ions are known to depolymerize f-Actin and affect the cadherin−catenin complex,[24] and our images suggest that this is exactly what happens if the cells are exposed to QDs, supporting the hypothesis that indeed cadmium ions are released from the multishell QDs. The cell's cortical Actin ring is less pronounced than in controls, and nanoparticles seem to arrange along fibers. Notably, QDs, like gold particles, do not enter the nucleus.

Although nowadays the call for *in vivo* characterization of nanotoxicity is strong,[25] cell culture models are important for physiological and toxicological preclinical research; therefore, an approach comparing various assays on common model cell lines and standardized particles is desirable: for the latter case, gold particles seem to be an appropriate candidate since in many studies on different cells lines they are referred to be only slightly toxic, usually decreasing vitality from 10 to 20%. A comprehensive overview of cytotoxicity generated by carbon, gold, and semiconductor nanoparticles is given by Lewinski *et al.*[23] To date, however, impedance spectroscopy has only sparsely been applied to assess particle toxicity and only once recently to address nanoparticles toxicity in focus.[26] Male *et al.* herein found an IC_{50} toxicity for semiconductor nanoparticles without multishell arrangement, by montoring IZI as a function of time, to lay around 154 nM, indicating that our IC_{50} value of 300 nM found is due to an enhanced diffusion barrier by the multishell arrangement. Ceriotti *et al.*[27] report on cobalt-based metallic nanoparticles, which showed toxicity at concentrations larger than 300 μM after 24 h, which is 500 times higher than the toxic dose QDs and 400 times higher than the dose of gold particles used in our study. Krol and co-workers investigated the toxicity of gold nanoparticles with four-layer PAH coating by means of impedance spectroscopy. The authors found strong toxicity of particles after 17 h.[28] The concentration regime at which the particles showed toxicity was in the range of 2000 μg/mL, considerably lower than the concentration regime in which CTAB-coated rods are cytotoxic. Another widely used approach is to monitor cell motility and/or toxicity of nanoparticles *via* optical microscopy. Parak *et al.*[29] found quantum dots with $CdSe/ZnS/SiO_2$ composition of 8 and 16 nm diameter to be nontoxic to the two epithelial cell lines MDA-MB 231 and MCF-10. The particles were placed at high density on the substrate and internalized to a great degree, resulting in perinuclear arrangement. Thereby, cell motility could be observed *via* migratory pathways comparable to the phagokinetic tracking assay. By means of DIC microscopy, Kirchner *et al.*[18] determined the toxic concentration for MPA-coated QDs with multishell structure to be 0.65 μM. This is in good accordance with our ECIS micromotion assay, which provided values in the range of 0.3 μM, while the MTS test reported a concentration of 2 μM. The examples clearly support our conclusion that the sensitivity of micromotion to the exposure of nanoparticles is higher than that of conventional cytotoxicity assays.

Impedance spectroscopy is a versatile tool to quantify cell viability. Apart from micromotion, which measures the motility of already adherent cells, cell−cell contact and adhesion of cells can be investigated by AC impedance analysis. For instance, Zimmerhackl *et al.* measured the TER of MDCK cells to determine the cytotoxic concentration of cadmium ions applied from the basolateral side.[24] The authors found an IC_{50} larger than 12.5 μM, which is a factor of 3 higher than the value we determined by our micromotion assay. For comparison, Ceriotti *et al.*[27] found an inhibition concentration of 34 μM after 24 h exposure to cadmium ions by measuring the impedance upon adhesion of fibroblasts. However, combination with classical cytotoxicity assays and advanced optical single particle microscopy is necessary to elucidate the fate of the nanoparticles, as done by Shukla *et al.*[30] Due to the fact that not all cells display a measurable TER and the influence of nanoparticles on tight junctions varies between particles or cells, micromotion is a more appropriate and universal approach to determine toxicity rather than monitoring of the TER.

Particle toxicity is a function of size, shape, and most importantly surface functionalization.[31] The surface coating of particles influences their uptake and fate once they entered the cell. In the present work, we found by recording the micromotion of confluent epithelial cells that PEGylation increases the biocompatibil-

ity substantially. Dark-field microscopy in conjunction with immunofluorescence of cytoskeleton filaments shows that CTAB-coated particles enter cells with high efficiency, while PEGylation suppresses the particle uptake of cells significantly. However, even at particle concentrations that lead to accumulation of PEGylated gold nanorods within the cytosol, cytotoxicity measured by micromotion is negligible.

CONCLUSIONS

Micromotion measured by impedance analysis provides a noninvasive and versatile tool to assess the toxicity of nanoparticles with high sensitivity. Compared to conventional cytotoxicity tests, micromotion detects minute changes in cell viability already at very low particle concentrations without the need for colorimetric or fluorescent labels and in real-time. It provides dynamic IC_{50} values, which increase our insight into mechanisms of particle−cell interaction. Dark-field microscopy of gold nanorods is the ideal supplement to micromotion since it allows visualizing the location of particle also in a noninvasive manner. We found that, even when QDs are capped and stabilized against Cd^{2+} diffusion with an external ZnS shell in a 6-fold monolayer arrangement, they are toxic, while PEGylated nanorods are esentially harmless to adherent epithelial cells.

METHODS

ECIS-Based Micromotion Experiments and Noise Analysis. A homemade ECIS system was employed, consisting of a lock-in amplifier (SR830, SRS, Inc., Sunnyvale, CA) with an internal oscillator, a multiplexer with analogue switches for automatic, consecutive addressing of individual wells on the electrode array, and a PC for experiment control and data storage. The ECIS electrode arrays (type 8W1E) purchased from Applied Biophysics (Troy, USA) consist of eight separate wells, each holding one gold microelectrode of 250 μm diameter and a large (7 × 46 mm^2) counter electrode. In our ECIS setup, a 1 V AC signal is applied to the system through a 1 MΩ series resistor, and the in- and out-of-phase voltages across the electrodes are recorded at 4 kHz at a sampling rate of 1 Hz. For micromotion recordings, the in-phase voltage, which is directly proportional to the real part of the complex impedance, was used for further analysis as it provides the most sensitive readout. The applied constant current of 1 μA amplitude is noninvasive to the cell layer.

Besides micromotion recordings at one fixed frequency, we also monitored changes in the barrier function of the adherent MDCK cell layer when exposed to the NPs. Barrier function can be most easily expressed by means of the so-called transepithelial electrical resistance (TER), which is a direct measure for the ionic permeability of the cell−cell junctions. TER values were extracted from frequency-resolved impedance readings (10−10^4 Hz) and subsequent equivalent circuit modeling according to the procedures described by Wegener *et al.*[15] In contrast to the most commonly applied approach to determine TER values, there is no need to grow the cells on permeable filter substrates for the measurement. Micromotion and TER readings can be performed on one and the same cell layer with just different ECIS measurement modes.

As suggested by Giaever and co-workers, micromotion data, which are essentially a time series of resistance fluctuations, were subject to Fourier transformation after subtracting a linear trend (Figure 2A).[32] A linear fit of the low frequency part of the power density spectra provided slopes from −2.1 to −2.7 s^{-2} for living cells (Figure 2B). Time courses of the slope representing micromotion activity and the TER are recorded as a function of particle type and concentration, exemplary depicted for 1.38 × 10^{11} p/mL gold rods and 7.5 × 10^{13} p/mL QDs (Figure 2C,D).

Cell Culture Conditions and Measurement Procedures. MDCK II cells are maintained in Earle's minimum essential medium supplemented with 4 mM glutamine, 100 μg/mL of both penicillin and streptomycin (purchased by Biochrom, Berlin, Germany), 10% (v/v) fetal calf serum (PAA Laboratories GmbH, Cölbe, Germany) and stored in incubators (HERA cell 150, Heraeus, Germany) with a 5% CO_2 atmosphere. Cells are subcultured weekly after reaching confluence by washing with PBS, followed by trypsinization and centrifugation at 110*g*. Counting is carried out using a Neubauer chamber, and viability is determined using trypan blue exclusion. For the measurements, cells are seeded in the 8-well electrode arrays that had been preincubated with HEPES buffered full medium for 2 h and are then transferred to an incubator (CO_2Cell, MMM, Germany) set to 37 °C and 5% CO_2. The electrode array is connected to the homemade ECIS setup to allow for continuous ECIS recordings. Seeding density was adjusted to 6 × 10^5 cells per well to reach confluence in seven of the eight wells, and the remaining well served as a cell-free reference filled with an equal amount of medium only. Exchange of medium with medium containing nanoparticles or pure Cd^{2+} and cetyl triammonium bromide (CTAB) detergent solution is carried out 15−24 h after seeding.

Nanoparticle Preparation. Gold nanorods are prepared using the seed growth method as reported by Nikoobakht *et al.* and Jana *et al.*[33,34] Briefly, seeds are prepared by reducing 10 mL of an aqueous solution containing 0.25 mM gold tetrachloride (HAuCl4) in 0.1 M hexadecyltrimethylammonium bromide (CTAB, Sigma) adding 0.6 mL of 0.01 M sodium borohydride ($NaBH_4$). Fifteen microliters of this seed solution is added to 10 mL of a growth solution consisting of 0.5 mM $HAuCl_4$ and 0.08 mM silver nitrate in 0.1 M CTAB mixed with 70 μL of 0.0788 M ascorbic acid. A strong color change indicates the formation of the gold nanorods after about 20 min, resulting in a stable suspension of CTAB-coated nanorods. In a further step, for stabilization in various solvents and biofunctionalization, either carboxyl- or amino-terminated PEG-thiol (Iris Biotech) is covalently grafted on the nanorods surface as described in detail by Pierrat *et al.*[35] Gold particles are freshly prepared, centrifuged two times, and resuspended in HEPES buffered complete medium to gain stock solutions of 6.6 × 10^{11} p/mL; concentrations from twice the stock to 4.6 × 10^9 have been used. CdSe/CdS/ZnCdS/ZnS multishell QDs with good quantum yield are prepared as described previously.[36] A mercaptopropionic acid (MPA) coating, needed to change the surface polarity from hydrophobic to hydrophilic, is added as the outermost layer. The aqueous stock solutions of 6 × 10^{14} or 6 × 10^{15} p/mL at basic pH of 10.8 have been diluted in HEPES buffered complete medium to the desired concentrations ranging from 6 × 10^{11} to 3 × 10^{14} p/mL and pH 7.4. In control experiments, $Cd(Ac)_2$ solution and pure CTAB detergent dissolved in culture medium are applied in the concentration range from 0.16 to 31.25 μM for $Cd(Ac)_2$ and 0.625 to 31.25 μM for CTAB.

Cytotoxicity Assay, Immunochemistry, Dark-Field and Fluorescence Microscopy. The MTS cytotoxicity test has been applied according to the manufacturers' protocol. In brief, cells are grown to a predetermined optimal number of 12 000/well in a 96-well plate and were subsequently incubated with eight different concentrations of nanoparticles or toxins for 24 or 48 h. Washing is carried out three times with PBS^{+2} and full medium before adding the MTS agent to remove the NPs or air bubbles that might disturb the photometric assay. Control experiments were carried out using cell-free wells but also fully vital cells that were not exposed to the NPs. The cells are incubated with the tetrazolium educt for 45 min. Absorbance is determined subsequently using a 96-well plate photometer at a wavelength of 490 nm. The color change is a direct measure of the cell's metabolic activity

due to the reduction of MTS educts to formazan by mitochondrial dehydrogenases. Experiments are performed three times.

Immunostaining and fluorescence microscopy are applied to monitor alterations in the cell cytoskeleton upon nanoparticle exposure. Therefore, MDCK II cells grown to confluence on petri dishes are incubated with nanoparticles or pure Cd^{2+} and CTAB detergent solution for time intervals and cell numbers similar to the ECIS measurements. After washing with PBS, fixation is carried out by immersing the cells into a −20 °C cold acetone/methanol mixture (1:1 vol %) for 10 min. Afterward, the cells are washed three times with PBS, unspecific binding sites blocked with FCS, and incubation in staining solutions carried out according to the manufacturer's recommendation: Alexa Fluor 488 phalloidin (invitrogen, Paisley, UK) is used for f-Actin staining, Alexa Fluor-conjugated IgG_1 anti-β-tubulin (BD Bioscience, Heidelberg, Germany) from mouse for labeling microtubules, 4′-6-diamidino-2-phenyindole (DAPI, Sigma-Aldrich, Seelze) for nucleus and DNA labeling, and polyclonal IgG_1 mouse antibody (Zymed Gmbh, Munich) followed by Alexa Flour-conjugated goat-antimouse IgG_1 antibody (BD Bioscience, Heidelberg, Germany) are used for staining tight junctions (ZO1 staining). Staining is carried out for 30 min at room temperature, and cells are then washed and examined under an upright Olympus fluorescence microscope (Olympus BX51, 40× water immersion, Germany), equipped with a color camera (3 MP) and a dark-field condensor. Distribution of gold nanorods is visualized by dark-field microscopy, while semiconductor QDs are located with the fluorescence microscope.

Acknowledgment. Financial support was granted by the graduate school of excellence MAINZ and the German Science Foundation (DFG) through the SPP 1313 Bio-Nano-Responses program.

REFERENCES AND NOTES

1. Harrison, R. Nanoparticles in the Atmosphere. In *Nanotechnology—Consequences for Human Health and the Environment*; Hester, R. E., Harrison, R. M., Eds.; RCS Publishing: Cambridge, 2007; pp 35−48.
2. Long, T. C.; Saleh, N.; Tilton, R. D.; Lowry, G. V.; Veronesi, B. Titanium Dioxide (P25) Produces Reactive Oxygen Species in Immortalized Brain Microglia (BV2): Implications for Nanoparticle Neurotoxicity. *Environ. Sci. Technol.* **2006**, *40*, 4346–4352.
3. Hodgson, E.; LeBlanc, G. A.; Meyer, S. A.; Smart, R. C. Introduction to Biochemical and Molecular Methods in Toxicology. In *A Textbook of Modern Toxicology*; Hodgson, E., Ed.; John Wiley & Sons, Inc.: Hoboken, NJ, 2004; pp 13−22.
4. Giaever, I.; Keese, C. R. Monitoring Fibroblast Behaviour in Tissue-Culture with an Applied Electric-Field. *Proc. Natl. Acad. Sci. U.S.A.* **1984**, *81*, 3761–3764.
5. Xiao, C.; Lachance, B.; Sunahara, G.; Luong, J. H. T. An In-Depth Analysis of Electric Cell-Substrate Impedance Sensing to Study the Attachment and Spreading of Mammalian Cells. *Anal. Chem.* **2002**, *74*, 1333–1339.
6. Ceriotti, L.; Ponti, J.; Colpo, P.; Sabbioni, E.; Rossi, F. Assessment of Cytotoxicity by Impedance Spectroscopy. *Biosens. Bioelectron.* **2007**, *22*, 3057–3063.
7. Arndt, S.; Seebach, J.; Psathaki, K.; Galla, H. J.; Wegener, J. Bioelectrical Impedance Assay to Monitor Changes in Cell Shape During Apoptosis. *Biosens. Bioelectron.* **2004**, *19*, 583–594.
8. McCoy, M. H.; Wang, E. Use of Electric Cell-Substrate Impedance Sensing as a Tool for Quantifying Cytopathic Effect in Influenza A Virus Infected MDCK Cells in Real-Time. *J. Virol. Methods* **2005**, *130*, 157–161.
9. Giaever, I.; Keese, C. R. Micromotion of Mammalian-Cells Measured Electrically. *Proc. Natl. Acad. Sci. U.S.A.* **1991**, *88*, 7896–7900.
10. Lo, C. M.; Keese, C. R.; Giaever, I. Monitoring Motion of Confluent Cells in Tissue-Culture. *Exp. Cell Res.* **1993**, *204*, 102–109.
11. Lovelady, D. C.; Richmond, T. C.; Maggi, A. N.; Lo, C. M.; Rabson, D. A. Distinguishing Cancerous from Noncancerous Cells through Analysis of Electrical Noise. *Phys. Rev. E* **2007**, *76*, 1–10.
12. Huff, T. B.; Tong, L.; Zhao, Y.; Hansen, M. N.; Cheng, J. X.; Wei, A. Hyperthermic Effects of Gold Nanorods on Tumor Cells. *Nanomed.* **2007**, *2*, 125–132.
13. Vashist, S. K. T. R.; Bajpai, R. P.; Mohan, B.; Raiteri, R. Review of Quantum Dot Technologies for Cancer Detection and Treatment. *Nanotech. Online* **2006**, *2*, 1–14.
14. Michalet, X.; Pinaud, F. F.; Bentolila, L. A.; Tsay, J. M.; Doose, S.; Li, J. J.; Sundaresan, G.; Wu, A. M.; Gambhir, S. S.; Weiss, S. Quantum Dots for Live Cells, *In Vivo* Imaging, and Diagnostics. *Science* **2005**, *307*, 538–544.
15. Wegener, J.; Sieber, M.; Galla, H. J. Impedance Analysis of Epithelial and Endothelial Cell Monolayers Cultured on Gold Surfaces. *J. Biochem. Biophys. Methods* **1996**, *32*, 151–170.
16. Hillaireau, H.; Couvreur, P. Polymeric Nanoparticles as Drug Carrier. In *Polymers in Drug Delivery*; Uchegbu, I. F., Schatzlein, A. G., Eds.; Taylor and Francis: New York, 2006; pp 101−110.
17. Goodman, C. M.; McCusker, C. D.; Yilmaz, T.; Rotello, V. M. Toxicity of Gold Nanoparticles Functionalized with Cationic and Anionic Side Chains. *Bioconjugate Chem.* **2004**, *15*, 897–900.
18. Kirchner, C.; Liedl, T.; Kudera, S.; Pellegrino, T.; Javier, A. M.; Gaub, H. E.; Stolzle, S.; Fertig, N.; Parak, W. J. Cytotoxicity of Colloidal CdSe and CdSe/ZnS Nanoparticles. *Nano Lett.* **2005**, *5*, 331–338.
19. Wei, X. L.; Mo, Z. H.; Li, B.; Wei, J. M. Disruption of HepG2 Cell Adhesion by Gold Nanoparticle and Paclitaxel Disclosed by *In Situ* QCM Measurement. *Colloids Surf., B* **2007**, *59*, 100–104.
20. Pan, Y.; Neuss, S.; Leifert, A.; Fischler, M.; Wen, F.; Simon, U.; Schmid, G.; Brandau, W.; Jahnen-Dechent, W. Size-Dependent Cytotoxicity of Gold Nanoparticles. *Small* **2007**, *3*, 1941–1949.
21. Lovelady, D. C.; Friedman, J.; Patel, S.; Rabson, D. A.; Lo, C. M. Detecting Effects of Low Levels of Cytochalasin B in 3T3 Fibroblast Cultures by Analysis of Electrical Noise Obtained From Cellular Micromotion. *Biosens. Bioelectron.* **2008**, doi:10.1016/j.bios.2008.09.033.
22. Arndt, S.; Seebach, J.; Psathaki, K.; Galla, H. J.; Wegener, J. Bioelectrical Impedance Assay to Monitor Changes in Cell Shape During Apoptosis. *Biosens. Bioelectron.* **2004**, *19*, 583–594.
23. Lewinski, N.; Colvin, V.; Drezek, R. Cytotoxicity of Nanoparticles. *Small* **2008**, *4*, 26–49.
24. Zimmerhackl, L. B.; Momm, F.; Wiegele, G.; Brandis, M. Cadmium is More Toxic to LLC-PK1 Cells Than to MDCK Cells Acting on the Cadherin-Catenin Complex. *Am. J. Physiol.* **1998**, *44*, F143–F153.
25. Fischer, H. C.; Chan, W. C. Nanotoxicity: The Growing Need for *In Vivo* Study. *Curr. Opin. Biotechnol.* **2007**, *18*, 565–571.
26. Male, K. B.; Lachance, B.; Hrapovic, S.; Sunahara, G.; Luong, J. H. T. Assessment of Cytotoxicity of Quantumdots and Gold Nanoparticles using Cell-Based Impedance Spectroscopy. *Anal. Chem.* **2008**, *80*, 5487–5493.
27. Ceriotti, L.; Ponti, J.; Broggi, F.; Kob, A.; Drechsler, S.; Thedinga, E.; Colpo, P.; Sabbioni, E.; Ehret, R.; Rossi, F. Real-Time Assessment of Cytotoxicity by Impedance Measurement on a 96-Well Plate. *Sens. Actuators, B* **2007**, *123*, 769–778.
28. Chanana, M.; Gliozzi, A.; Diaspro, A.; Chodnevskaja, I.; Huewel, S.; Moskalenko, V.; Ulrichs, K.; Galla, H. J.; Krol, S. Interaction of Polyelectrolytes and Their Composites with Living Cells. *Nano Lett.* **2005**, *5*, 2605–2612.
29. Parak, W. J.; Boudreau, R.; Le Gros, M.; Gerion, D.; Zanchet, D.; Micheel, C. M.; Williams, S. C.; Alivisatos, A. P.; Larabell, C. Cell Motility and Metastatic Potential Studies Based on Quantum Dot Imaging of Phagokinetic Tracks. *Adv. Mater.* **2002**, *14*, 882–885.

30. Shukla, R.; Bansal, V.; Chaudhary, M.; Basu, A.; Bhonde, R. R.; Sastry, M. Biocompatibility of Gold Nanoparticles and Their Endocytotic Fate Inside the Cellular Compartment: A Microscopic Overview. *Langmuir* **2005**, *21*, 10644–10654.
31. Hoshino, A.; Fujioka, K.; Oku, T.; Suga, M.; Sasaki, Y. F.; Ohta, T.; Yasuhara, M.; Suzuki, K.; Yamamoto, K. Physicochemical Properties and Cellular Toxicity of Nanocrystal Quantum Dots Depend on Their Surface Modification. *Nano Lett.* **2004**, *4*, 2163–2169.
32. Sapper, A.; Wegener, J.; Janshoff, A. Cell Motility Probed by Noise Analysis of Thickness Shear Mode Resonators. *Anal. Chem.* **2006**, *78*, 5184–5191.
33. Nikoobakht, B.; El-Sayed, M. A. Preparation and Growth Mechanism of Gold Nanorods (NRs) Using Seed-Mediated Growth Method. *Chem. Mater.* **2003**, *15*, 1957–1962.
34. Jana, N. R.; Gearheart, L.; Murphy, C. J. Seed-Mediated Growth Approach for Shape-Controlled Synthesis of Spheroidal and Rod-Like Gold Nanoparticles Using a Surfactant Template. *Adv. Mater.* **2001**, *13*, 1389–1393.
35. Pierrat, S.; Zins, I.; Breivogel, A.; Sönnichsen, C. Self-Assembly of Small Gold Colloids with Functionalized Gold Nanorods. *Nano Lett.* **2007**, *7*, 259–263.
36. Xie, R. G.; Kolb, U.; Li, J. X.; Basché, T.; Mews, A. Synthesis and Characterization of Highly Luminescent CdSe-Core CdS/Zn0.5Cd0.5S/ZnS Multishell Nanocrystal. *J. Am. Chem. Soc.* **2005**, *127*, 7480–7488.